A facile approach to fabricate self-assembled magnetic nanotheranostics for drug delivery and imaging

Ye Yuan[a,b], **Yixuan He**[#b], **Ruonan Bo**[#b], **Zhao Ma**[b], **Zhongling Wang**[b], **Lijie Dong**[a], **Tzu-yin Lin**[c], **Xiangdong Xue**[b], and **Yuanpei Li**[b]

[a.]School of Materials Science and Engineering, Wuhan University of Technology, Luoshi Road 122, Wuhan, 430070,P.R. China

[b.]Department of Biochemistry and Molecular Medicine, UC Davis Comprehensive Cancer Center, University of California Davis, Sacramento, CA 95817, USA, xxdxue@ucdavis.edu, lypli@ucdavis.edu

[c.]Division of Hematology/Oncology, Department of Internal Medicine, University of California Davis, Sacramento, CA 95817, USA

[#] These authors contributed equally to this work.

Abstract

Superparamagnetic iron oxide (SPIO) nanoparticles were extensively employed for theranostic applications, due to their good biocompatibility and excellent magnetic resonance imaging (MRI) properties. However, these particles typically require surface modification due to their hydrophobic surfaces caused by the oil-phase surfactants used in the fabrication and the drug loading on their surface is usually limited. Here, we provided a novel and facile approach to conveniently perform surface modification of SPIO while simultaneously loading a large amount of drug. By synthesizing an amphiphilic irinotecan-based compound, which hydrophobic tail enabled to insert into the SPIOs assembly, an excellent SPIO-based theranostic nanomedicine (SPIO@IR) was formed. The SPIO@IR can not only extensively improve the drug efficacy, but also enable to visualize themselves by MRI in the biological system.

Chemotherapy is one of the most commonly used approaches for cancer therapy. However, the chemotherapeutic drugs have less selectivity, which not only kill the cancer cells, but also damage the normal cells, thus lead to severe side effects. To overcome these side effects, various nanocarriers were exploited to deliver the chemotherapeutic agents to the tumour sites. These drug delivery systems include polymeric micelles for encapsulating hydrophobic drugs[1-5], liposomes or vesicles for carrying both hydrophilic and hydrophobic drugs[6-9], or drug-drug amphiphiles for self-assembling into nanoparticles (NPs)[10, 11]. With various developed nanoscale drug delivery systems (NDDSs)[12-14], the chemotherapeutic drugs that are delivered by NDDS could selectively accumulate in tumour tissue due to the enhanced permeability and retention (EPR) effect[15] and enable efficient uptake by tumour cells due to the endocytosis or membrane fusion.

Conflicts of interest

There are no conflicts to declare.

Nanotheranostics are NDDSs which integrate therapeutic and diagnostic features simultaneously. With this strategy, a great variety of nanoplatforms were used to accomplish the imaging functionalities, such as near-infrared fluorescence imaging (NIRFI),[16] magnetic resonance imaging (MRI),[11,17-19] computed tomography (CT),[20, 21] positron emission tomography (PET),[22, 23] ultrasonic imaging,[24] or photoacoustic imaging (PAI)[25] for cancer monitoring and diagnosis.[26-28] For MR imaging, superparamagnetic iron oxide (SPIO) NPs were extensively employed as T_2 contrast agent for T_2-weighted MR imaging.[15, 29] However, the highly uniform SPIOs usually showed hydrophobic surfaces attributed to the oil-phase surfactants used in their fabrication, which largely hindered their biological applications. Therefore, a facile method that can effectively turn the synthesized NPs in oil-phase into water-soluble ones is a prerequisite. By proper modification to the surface, the NPs become water soluble because the introduced groups might become cations and/or anions in the water solution. One strategy involves physically encapsulating NPs within organic molecules or polymers with hydrophilic groups,[30-32] or inorganic shells like silicon dioxide.[33-35] Notably, such strategy resulted in NPs with large diameter, which may limit their biological applications. Moreover, these methods need to take extra steps to introduce the therapeutic agents to achieve the theranostic functionalities. The other strategy is called ligand exchange. This ligand exchange strategy offers a practical and convenient method for surface modification of SPIO NPs by the association reaction between transition metal and organic group,[36-38] which could endow the final NPs with stability as well as different solubility.

However, the approaches to deliver the drug using theranostic NPs with the properties of diagnosis, as well as therapy, were always complicated and expensive. A tedious process of synthesis is typically involved, which causes difficult for bulk production. To overcome this limitation, we designed a simple yet efficient method to fabricate a hydrophobic SPIO based nanoparticle with the chemo drug inserted on the surface while transforming it into a water-soluble one. This nanoparticle has better drug efficacy compares to the free drug; besides of that, this simply-made nanoparticle is a potential agent for MR imaging. The way we used to assemble this nanoparticle with surface modification is neither polymer encapsulation nor ligand exchange. To the best of our knowledge, this is a type of new method to simply modify hydrophobic nanoparticles into water-soluble ones while simultaneously loading high level of drugs. This facile approach is generally applicable for other hydrophobic inorganic nanoparticles and drug conjugates.

In our work, an amphiphilic lauric acid-irinotecan (LA-IR) prodrug (Figure 1A) was synthesized by directly conjugating lauric acid and irinotecan through simple esterification. The chemical structures were confirmed by MALDI-TOF-MS (Figure S1) and ^{1}H nuclear magnetic resonance spectroscopy (^{1}H NMR) (Figure S2). To fabricate SPIO-based theranostic nanomedicine (SPIO@IR), the amphiphilic LA-IR molecules were employed as surfactant to turn the hydrophobic SPIO hydrophilic. Briefly, 0.5 mg hydrophobic SPIO and 5 mg LA-IR were dissolved in 400 μL of tetrahydrofuran (THF), and slowly added into 1 mL deionized water dropwise under vigorous string. The stirring was kept for overnight till the THF was completely evaporated. This yielded a stable solution of nanoformulated LA-IR inserted SPIO prodrug with a final concentration of 0.24 mg/mL SPIO and 5mg/mL LA-IR. The drug to SPIO mass ratio was 15.9, which is a dramatic enhancement compared with

other SPIO-drug systems.[39-41] To verify that LA-IR was inserted into the surface of hydrophobic SPIO instead of self-assembled into nanoparticles themselves, their fluorescence spectra were obtained (Figure 1B). The fluorescence intensity of SPIO@IR exhibited only slight changes in water compared to that in DMSO (good solvent) at the same concentration, indicating that the IR molecules did not form aggregation on the surface of the SPIO, but were well-dispersed. This result was consistent with the formation of inserted nanostructure, in which the fluorescence of LA-IR did not reduce much by the aggregation-caused quenching (ACQ) effect.[42]

The morphology and hydrodynamic size of SPIO@IR were investigated by transmission electron microscopy (TEM) and dynamic light scattering (DLS), respectively. The self-assembled SPIO@IR was stable and clear, and well dispersed in aqueous solution. The hydrodynamic size of SPIO@IR was 117 nm as measured by DLS (Figure 1C) with the polydispersity index (PDI) of 0.169, which demonstrated that the SPIO@IR nanoparticles are quite homogeneous. The stability of SPIO@IR was evaluated by DLS in aqueous solution. As shown in Figure S4, the size distribution of SPIO@IR exhibited imperceptible change and enabled to keep stable in size for more than 20 days. The stability indicated that SPIO@IR could maintain high stability in aqueous solution, which will be beneficial for biological applications in the future. TEM were used to observe the morphologies, which revealed a group of 20 nm hydrophobic SPIOs aggregated into a bigger iron oxide nanosphere (Figure 1D). The TEM measurements were consistent with the size distributions analysed by DLS. As shown in Figure 1D (inset image), the SPIO@IR could be well-dispersed in aqueous solution and showed blue fluorescence (came from irinotecan), suggesting that the hydrophobic SPIOs were successfully converted into hydrophilic nanotheranostics by our facile method. Besides, SPIO@IR nanoparticles were incubated with cell culture medium and 10% FBS for 24 h, and no precipitations were observed, indicating that the SPIO@IR nanoparticles were relatively stable, and no obvious IR-LA was detached from the surface of SPIO nanoparticles in serum. The surface charge of SPIO@IR NPs was tested to illustrate the surface status, which valued at around 63.4 mV (Figure S3), due to the IR on the surface of the NPs. The NPs with positive charge may exhibit better cellular uptake into cancer cells, due to electrostatic interactions with the negatively charged phospholipid membrane.[43, 44]

We posited the SPIO@IR NPs enabled to responsively release the IR under acidic pH circumstance, as the ester bond between LA and IR was acidic-liable[45]. Therefore, the pH-dependent drug release pattern of SPIO@IR was investigated; free IR was processed in parallel as a control. As shown in Figure S5, SPIO@IR in neutral pH showed only slight drug release within 8 h. In contrast, acidic pH (5.0) greatly expedited the drug release of SPIO@IR, which led to around 50% drug release of IR. The release rate of free IR could easily get to 100%, as the small molecules could go out of the dialysis membrane freely. The drug release indicated that SPIO@IR could effectively release the chemotherapeutic drug under acidic cell compartment, such as lysosomes.

The ability to shorten the T_2 transverse relaxation time of water protons was firstly measured to evaluate the imaging properties as well as diagnosability of SPIO@IR in comparison with hydrophilic SPIOs with carboxy surface coating prepared via ligand exchange method. The

iron concentrations in SPIO@IR and hydrophilic SPIO were determined using the 1,10-phenanthroline colorimetric method.[46] As shown in Figure 2, T_2-weighted MR images of SPIO@IR and hydrophilic SPIO ($[Fe_3O_4]$=0.01-0.06 mM) were evaluated on a 7.0 T MR scanner. The T_2-weighted images of hydrophilic SPIO and SPIO@IR with TR/TE of 800/45 ms were shown in the bottomright corner of Figure 2A and 2B respectively. The r_2 relaxivity values were calculated through the slope of the curve of $R_2(1/T_2)$ relaxation rates as a function of the iron concentration in mM. As seen in Figure 2A and Figure 2B, the r_2 of hydrophilic SPIO is 247.4 s^{-1} mM^{-1}, while that of SPIO@IR is 189.3 s^{-1} mM^{-1}. This result illustrated that the hydrophobic SPIO with LA-IR inserted on the surface still maintain the ability to shorten the T_2 transverse relaxation time of water protons. In consistence with the T_2 relaxation time, the T_2 mapping between hydrophilic SPIO and SPIO@IR showed similar trends in different iron concentrations (Figure 2C).

We next investigated the cellular uptake of SPIO@IR by using confocal laser scanning microscopy (CLSM). Human colorectal adenocarcinoma cells (HT-29) were incubated with free IR, SPIO@IR and the equivalent doses of hydrophilic SPIO for 3 h before observation. As shown in Figure 3, the SPIO@IR NPs-treated HT-29 cells exhibited the strongest Irinotecan fluorescence intensity (blue colour), reflecting the highest level of drug accumulation, while imperceptible fluorescence could be observed in the free irinotecan-treated cells. Figure 4A showed the flow cytometry results on cell uptake. SPIO@IR NPs were more readily to be taken up by the cancer cells than free irinotecan. Cancer cells treated with SPIO@IR were approximately 100 times higher than those treated with free drug in fluorescence intensity, which was consistent with the CLSM images. The accumulation of nano-formulation was higher than that of free drug, indicating the advantage of this strategy. In the CLSM images (Figure 3), SPIO@IR showed a region of bright blue fluorescence. We hypothesized that these regions corresponded to lysosomes. To test this, we stained the lysosomes with LysoTracker® Green. As shown in Figure 3, the blue irinotecan fluorescence in cells treated with SPIO@IR mostly co-localized with the green colour of LysoTracker®, revealing that such nanoparticles were co-localized with lysosomes. The lysosomes co-localization indicated that the SPIO@IR would accumulate in lysosomes once they have been uptaken, and the acidic pH value in this specific organelle enabled to cleave the ester bond, and thereby, triggered the drug release.

Then, the *in vitro* anti-tumour activities of SPIO@IR were tested in comparison with free IR. Firstly, we measured the cytotoxicity of nanoparticles to cancer cells. The overall cytotoxicity of SPIO@IR NPs was evaluated and compared with free IR and hydrophilic SPIO by MTS assays (Figure 4B). After incubating HT-29 cells with SPIO@IR and free IR containing equivalent concentrations of irinotecan (0.1-50 μM) along with hydrophilic SPIO with the equivalent iron concentration for 48 hrs, we found that hydrophilic SPIO showed nearly no toxicity to cancer cells. However, the nanotheranostics (SPIO@IR) showed much more cytotoxicity to HT-29 cells and had a much lower IC_{50} than free IR. Strikingly, at the highest concentration tested (50 μM), almost no toxicity of free IR was observed under our concentration range, which was in agreement with the reported work[47], while SPIO@IR NPs completely killed the cancer cells (Figure 4B). To verify this great enhancement of toxicity was not just caused by the positive surface charge, a normal prostatic epithelial cell line (PZ-HPV-7) was used. After incubating cells with SPIO@IR NPs for 48 hrs, there was a

significant difference in the viability between HT-29 cancer cells and PZ-HPV-7 normal cells at the concentration of 5 μM (IC_{50} of SPIO@IR in HT-29 cells) (Figure S6). At this concentration, almost half of the HT-29 cells were killed while all of the PZ-HPV-7 still alive. The dramatic enhancement of the cytotoxicity of the nanoparticles compared to free drug was hypothetically considered to be the consequence of significantly increased intracellular accumulation of the nanoformulation. Then, the cell apoptosis induced by SPIO@IR were evaluated by Annexin V FITC and PI Cy5.5 staining. The free IR and SPIO were employed as controls (Figure 4C). The results were analyzed based on the percentages of unstained cells (viable cells) and those with red fluorescence (necrotic cells), green fluorescence (apoptotic cells) and dual stained cells (late apoptosis). The assay was conducted following treatment of HT-29 cells with free IR, SPIO@IR and the equivalent doses of hydrophilic SPIO of 20 μM for 24 hrs. As shown in Figure 4C, the percentage of Annexin V positive cells increased from 6.32% of control to 63.5% when incubated with free IR and increased up to 91.3% with the presence of SPIO@IR NPs. The PI positive cells were increased from 4.71% of control to 32.67% in free IR group and reached 57.83% with SPIO@IR NPs. The results of the experiment revealed that SPIO@IR could significantly enhance the apoptosis induced by irinotecan. This hypothesis could also be proved by cell uptake results in Figure 4A. The cell uptake, cytotoxicity, and apoptosis studies all supported the superiorities of the nanotheranostics over free IR.

The diagnosis potential through MRI was demonstrated on HT-29 cells. The cells treated with free irinotecan, SPIO@IR NPs as well as the same dose of hydrophilic SPIO were dispersed in agarose gel to image on the 7 T MRI scanner. As shown in Figure 5, the MR signal enhancement (dark-contrast in the T_2-weighted image) was obviously observed in the MR images of HT-29 cells treated with SPIO@IR NPs compared with untreated one, free IR and the same dose of hydrophilic SPIO. The T_2 relaxation time was decreased greatly from 50 ms of the control to 35 ms of the one treated with SPIO@IR NPs. The minor difference in MR images between the control and the hydrophilic one is likely due to their limited uptake in cancer cells. The hydrophilic SPIO have carboxy group on the surface with relatively negative potential, and it is difficult for them to be taken up by cells.

Finally, the SPIO@IR nanoparticles were investigated on HT-29 bearing mice model for *in vivo* imaging, as the SPIO showed intrinsic MRI capacity. For the *in vivo* imaging, SPIO@IR nanoparticles were intravenous administrated into mice, the T_2 MRI signal of the nanoparticles were monitored at different timepoints. The hydrophilic SPIO was employed as control. As show in Figure 6, the mice were both showed long T_2 relaxation time before the administration of nanoparticles (Pre). In SPIO@IR nanoparticles treated mice, the T_2 MRI signal at the tumour site was gradually enhanced at 24h postinjection (Figure S8). In the hydrophilic SPIO treated mice, the T_2 MRI contrast at the tumour site enhanced at 4h of the postinjection and gradually faded at 24 h. The T_2 relaxation time at the tumour site decreased from 49 ms pre-injection to 36 ms at 24h post-injection of SPIO@IR nanoparticles. For the hydrophilic SPIO, the T_2 relaxation time at the tumour site decreased from 51 ms pre-injection to 33 ms at 4h postinjection and rebounded back to 49 ms at 24h post-injection (Figure S9). The MRI results supported that the SPIO@IR was stable enough in the blood circulation and enabled to take advantages of the EPR effect to selectively visualize the tumor tissues.

Conclusions

In conclusion, we have successfully developed a simple yet effective method to modify the hydrophobic SPIO NPs into hydrophilic particles as well as loading chemotherapeutic agent using an irinotecan-fatty acid conjugate. The water-soluble nanoparticles possessed superior drug loading capacity, and enhanced cytotoxicity against cancer cells compared to free irinotecan. Besides, these nanoparticles maintained the ability to be used as the MRI nanoprobe for cancer diagnosis. Based on this concept, we will design and develop other prodrug nano-formulation with the ability of MR imaging and cancer treatment. These nano-theranostics could be further improved by using polymers such as polyethylene glycol (PEG) to shield the positive charge on the surface for long circulation time while the polymers can be cleaved in the acidic tumour microenvironment to expose the positive charge for enhanced uptake into cancer cells. This strategy could potentially be used widely in the modification of hydrophobic inorganic nanotheranostics as well as the diagnosis probes to improve cancer management in the near future.

Supplementary Material

Refer to Web version on PubMed Central for supplementary material.

Acknowledgements

Notes and references

1. Li Y, Lin T.-y., Luo Y, Liu Q, Xiao W, Guo W, Lac D, Zhang H, Feng C, Wachsmann-Hogiu S, Walton JH, Cherry SR, Rowland DJ, Kukis D, Pan C and Lam KS, Nature Communications, 2014, 5, 4712.

2. Yang X, Xue X, Luo Y, Lin T.-y., Zhang H, Lac D, Xiao K, He Y, Jia B and Lam KS, Journal of Controlled Release, 2017, 261, 297–306. [PubMed: 28700898]

3. Louage B, Tack L, Wang Y and De Geest BG, Polymer Chemistry, 2017, 8, 5033–5038.

4. Ekkelenkamp AE, Elzes MR, Engbersen JF and Paulusse JM, Journal of Materials Chemistry B, 2018, 6, 210–235.

5. Emamzadeh M, Desmaele D, Couvreur P and Pasparakis G, Journal of Materials Chemistry B, 2018, DOI: 10.1039/C7TB02899G.

6. Nandwana V, Singh A, You MM, Zhang G, Higham J, Zheng T, Li Y, Prasad PV and Dravid V, Journal of Materials Chemistry B, 2018.

7. Caracciolo G, Nanoscale, 2018, 10, 4167–4172. [PubMed: 29450412]

8. Deng Y, Ling J and Li M-H, Nanoscale, 2018, 10, 6781–6800. [PubMed: 29616274]

9. Yang C, Zhang M and Merlin D, Journal of Materials Chemistry B, 2018, 6, 1312–1321. [PubMed: 30034807]

10. Huang P, Wang D, Su Y, Huang W, Zhou Y, Cui D, Zhu X and Yan D, Journal of the American Chemical Society, 2014, 136, 11748–11756. [PubMed: 25078892]

11. Xue X, Huang Y, Wang X, Wang Z, Carney RP, Li X, Yuan Y, He Y, Lin T.-y. and Li Y, Biomaterials, 2018, 161, 203–215. [PubMed: 29421556]

12. Lim E-K, Kim T, Paik S, Haam S, Huh Y-M and Lee K, Chemical reviews, 2014, 115, 327–394. [PubMed: 25423180]

13. Pérez-Herrero E and Fernández-Medarde A, European journal of pharmaceutics and biopharmaceutics, 2015, 93, 52–79. [PubMed: 25813885]

14. Debele TA, Peng S and Tsai H-C, International journal of molecular sciences, 2015, 16, 22094–22136. [PubMed: 26389879]

15. Estelrich J, Escribano E, Queralt J and Busquets MA, International journal of molecular sciences, 2015, 16, 8070–8101. [PubMed: 25867479]

16. Liu H-Y, Wu P-J, Kuo S-Y, Chen C-P, Chang E-H, Wu C-Y and Chan Y-H, Journal of the American Chemical Society, 2015, 137, 10420–10429. [PubMed: 26255823]

17. Na HB, Song IC and Hyeon T, Advanced materials, 2009, 21, 2133–2148.

18. Kim T, Momin E, Choi J, Yuan K, Zaidi H, Kim J, Park M, Lee N, McMahon MT and Quinones-Hinojosa A, Journal of the American Chemical Society, 2011, 133, 2955–2961. [PubMed: 21314118]

19. Johnson NJ, Oakden W, Stanisz GJ, Scott Prosser R and van Veggel FC, Chemistry of Materials, 2011, 23, 3714–3722.

20. Peng C, Zheng L, Chen Q, Shen M, Guo R, Wang H, Cao X, Zhang G and Shi X, Biomaterials, 2012, 33, 1107–1119. [PubMed: 22061490]

21. Wang H, Zheng L, Peng C, Guo R, Shen M, Shi X and Zhang G, Biomaterials, 2011, 32, 2979–2988. [PubMed: 21277019]

22. Yang X, Hong H, Grailer JJ, Rowland IJ, Javadi A, Hurley SA, Xiao Y, Yang Y, Zhang Y and Nickles RJ, Biomaterials, 2011, 32, 4151–4160. [PubMed: 21367450]

23. Sun Y, Yu M, Liang S, Zhang Y, Li C, Mou T, Yang W, Zhang X, Li B and Huang C, Biomaterials, 2011, 32, 2999–3007. [PubMed: 21295345]

24. Liu Z, Lammers T, Ehling J, Fokong S, Bornemann J, Kiessling F and Gatjens J, Biomaterials, 2011, 32, 6155–6163. [PubMed: 21632103]

25. Wang LV and Hu S, science, 2012, 335, 1458–1462. [PubMed: 22442475]

26. Kunjachan S, Ehling J, Storm G, Kiessling F and Lammers T, Chemical reviews, 2015, 115, 10907–10937. [PubMed: 26166537]

27. Li W and Chen X, Nanomedicine, 2015, 10, 299–320. [PubMed: 25600972]

28. Key J and Leary JF, International journal of nanomedicine, 2014, 9, 711. [PubMed: 24511229]

29. Vuong QL, Gillis P, Roch A and Gossuin Y, Wiley Interdisciplinary Reviews: Nanomedicine and Nanobiotechnology, 2017, 9.

30. Bhunia SK, Saha A, Maity AR, Ray SC and Jana NR, Scientific reports, 2013, 3, 1473. [PubMed: 23502324]

31. Guardia P, Riedinger A, Nitti S, Pugliese G, Marras S, Genovese A, Materia ME, Lefevre C, Manna L and Pellegrino T, Journal of Materials Chemistry B, 2014, 2, 4426–4434.

32. Palchoudhury S and Lead JR, Environmental science & technology, 2014, 48, 14558–14563. [PubMed: 25409536]

33. Zheng Y, Yang Z, Li Y and Ying JY, Advanced Materials, 2008, 20, 3410–3415.

34. Selvan ST, Biointerphases, 2010, 5, FA110–FA115. [PubMed: 21171704]

35. Ma Q, Serrano IC and Palomares E, Chemical Communications, 2011, 47, 7071–7073. [PubMed: 21617805]

36. Chen O, Zhao J, Chauhan VP, Cui J, Wong C, Harris DK, Wei H, Flan H-S, Fukumura D and Jain RK, Nature materials, 2013, 12, 445. [PubMed: 23377294]

37. Deng D, Cao J, Qu L, Achilefu S and Gu Y, Physical Chemistry Chemical Physics, 2013, 15, 5078–5083. [PubMed: 23450151]

38. Di Stasio F, Grim JQ, Lesnyak V, Rastogi P, Manna L, Moreels I and Krahne R, Small, 2015, 11, 1328–1334. [PubMed: 25335769]

39. Hola K, Markova Z, Zoppellaro G, Tucek J and Zboril R, Biotechnology advances, 2015, 33, 1162–1176. [PubMed: 25689073]

40. Bakandritsos A, Papagiannopoulos A, Anagnostou EN, Avgoustakis K, Zboril R, Pispas S, Tucek J, Ryukhtin V, Bouropoulos N and Kolokithas - Ntoukas A, small, 2012, 8, 2381–2393. [PubMed: 22549909]

41. Schleich N, Po C, Jacobs D, Ucakar B, Gallez B, Danhier F and Préat V, Journal of Controlled Release, 2014, 194, 82–91. [PubMed: 25178270]

42. Zhang C, Jin S, Xue X, Zhang T, Jiang Y, Wang PC and Liang X-J, Journal of Materials Chemistry B, 2016, 4, 3286–3291. [PubMed: 27239311]

43. Thompson DB, Villasenor R, Dorr BM, Zerial M and Liu DR, Chemistry & biology, 2012, 19, 831–843. [PubMed: 22840771]

44. Nakase I, Takeuchi T, Tanaka G and Futaki S, Advanced drug delivery reviews, 2008, 60, 598–607. [PubMed: 18045727]

45. Rijcken CJ, Snel CJ, Schiffelers RM, van Nostrum CF and Hennink WE, Biomaterials, 2007, 28, 5581–5593. [PubMed: 17915312]

46. Talelli M, Rijcken CJ, Lammers T, Seevinck PR, Storm G, van Nostrum CF and Hennink WE, Langmuir, 2009 25, 2060–2067. [PubMed: 19166276]

47. Tang W, Su G, Li J, Liao J, Chen S, Huang C, Liu F, Chen Q and Ye Y, International journal of oncology, 2014, 45, 995–1010. [PubMed: 24968890]

Author Manuscript

Author Manuscript

Author Manuscript

Author Manuscript
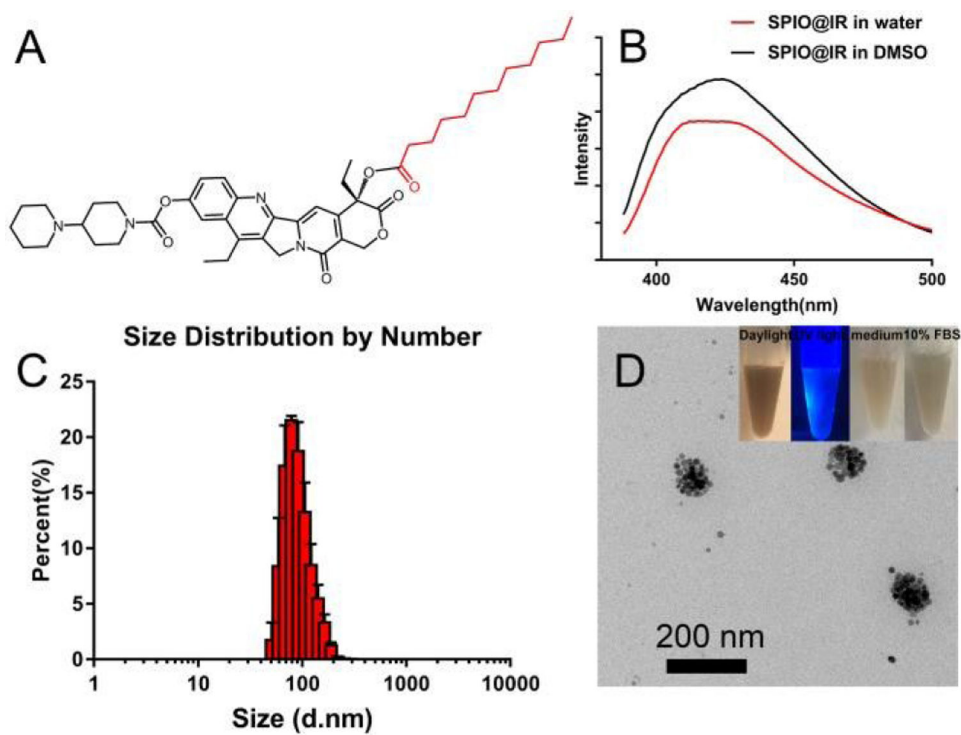
Fig.1.
A) Chemical structure of LA-IR; B) Fluorescence spectra of SPIO@IR in DMSO and in water at same concentration; C) DLS result of SPIO@IR in aqueous solution; D) TEM image of SPIO@IR (optical photos of SPIO@IR under daylight and UV light, and that in cell culture medium and in 10% FBS after 24h incubation were shown at right upper corner).
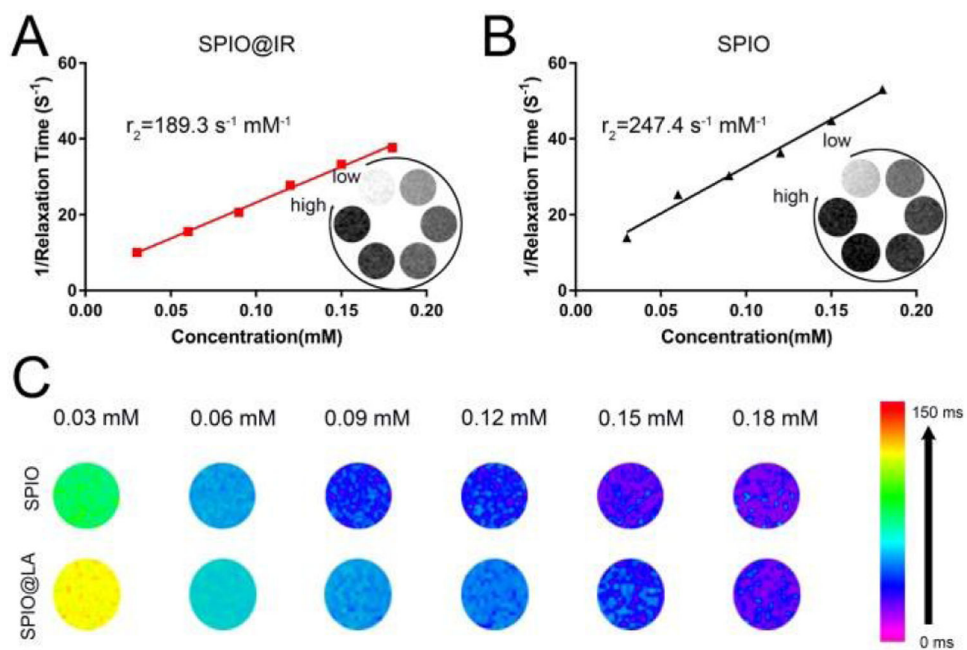
Fig.2.
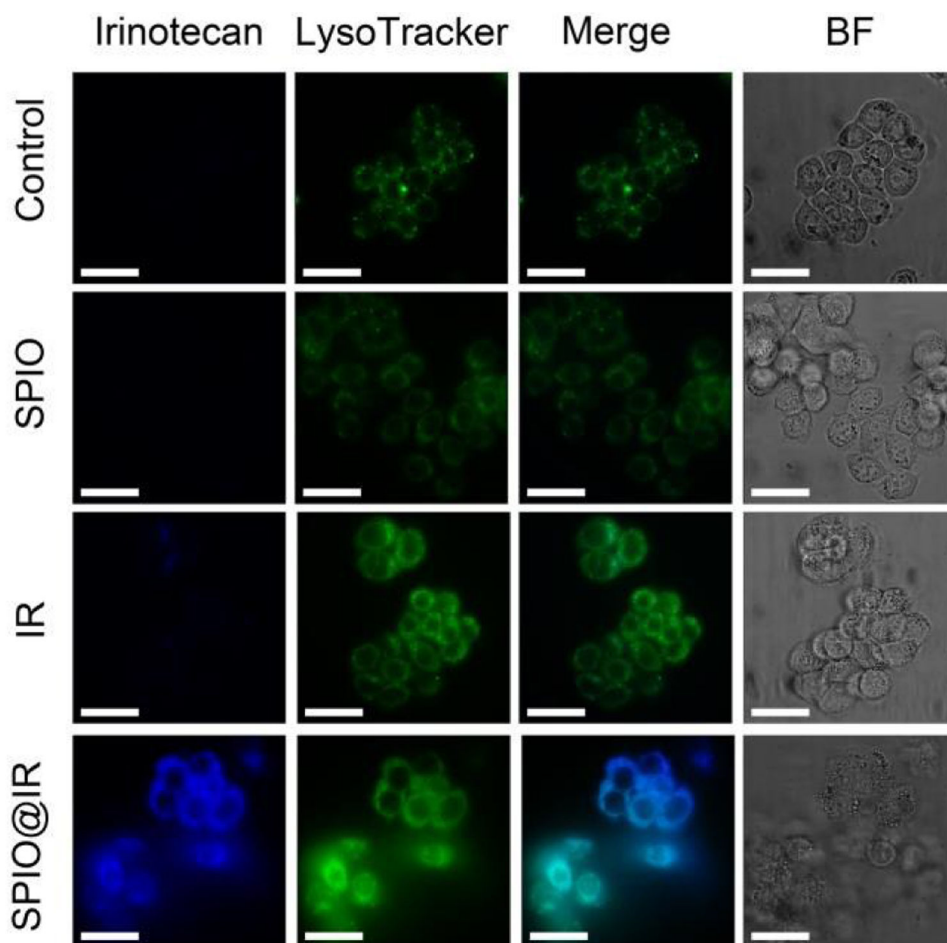Relaxivity measurements r_2 of (A) SPIO@IR and (B) hydrophilic SPIO; (C) T_2 mapping of SPIO@IR and hydrophilic SPIO.

Fig. 3.
CLSM images of cells treated with PBS, hydrophilic SPIO, free irinotecan and SPIO@LA (DAPI channel). Lysosomes were detected with LysoTracker® Green (FITC channel). Scale bars are 30 μm. BF, bright field images.
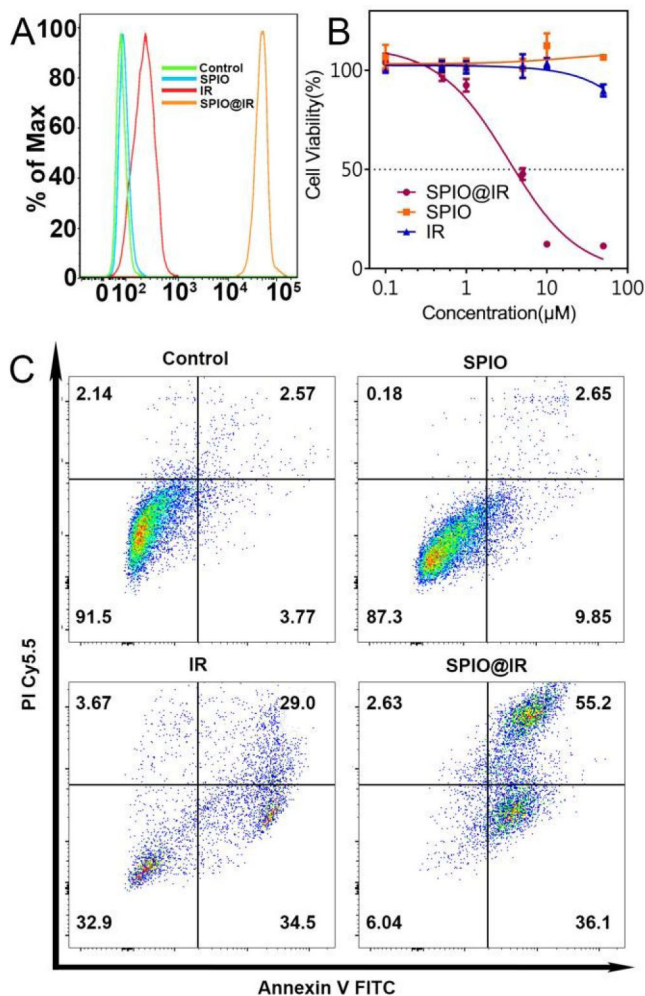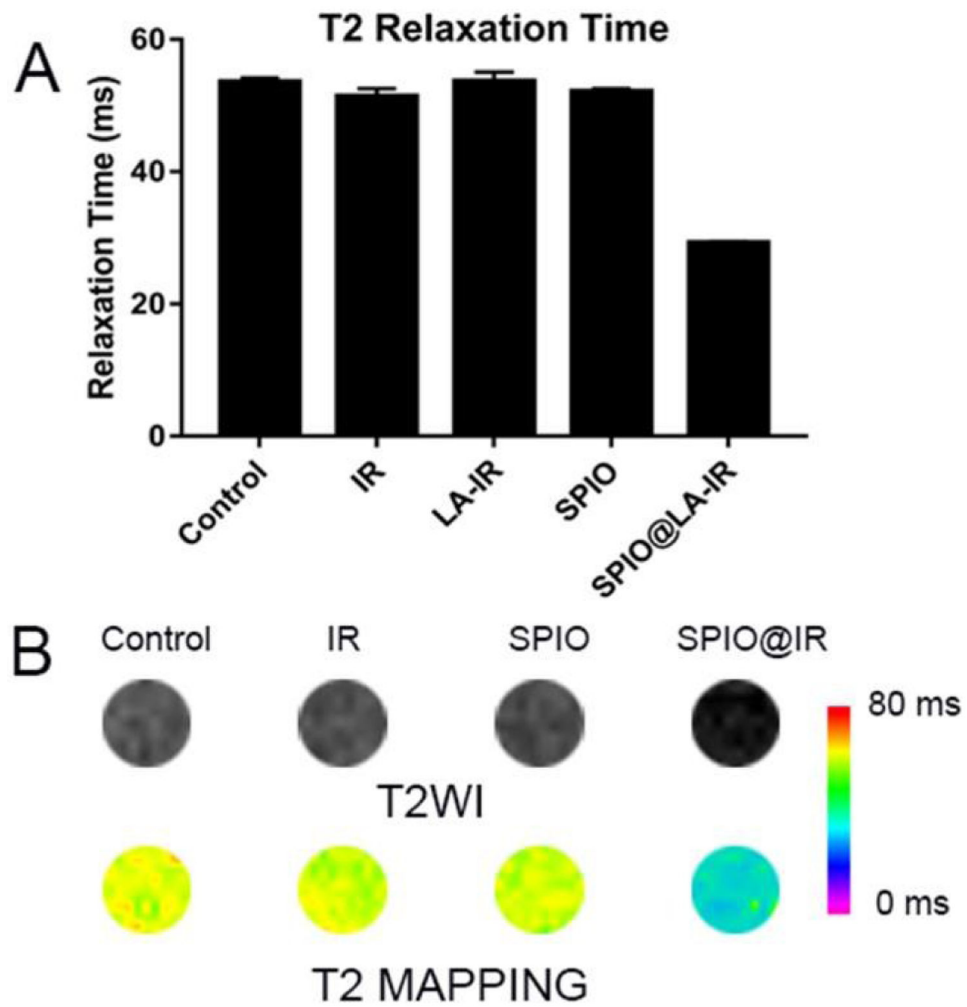
Fig.4.
A) Quantitative analysis of the uptake of hydrophilic SPIO, free irinotecan, and SPIO@IR by flow cytometry; B) *In vitro* cytotoxicity of hydrophilic SPIO, free Irinotecan, and SPIO@IR; C) Annexin V-FITC FACS apoptosis analysis of HT-29 cancer cells after treatment with PBS, hydrophilic SPIO, free irinotecan, and SPIO@IR.

Fig.5.
T_2 relaxation time (msec) (A), phantom based T_2-weighted images and pseudocolor processing of T_2 mapping (B) of HT-29 cells incubated with PBS, free Irinotecan, hydrophilic SPIO, and SPIO@IR in the same concentration of iron (1% agarose).
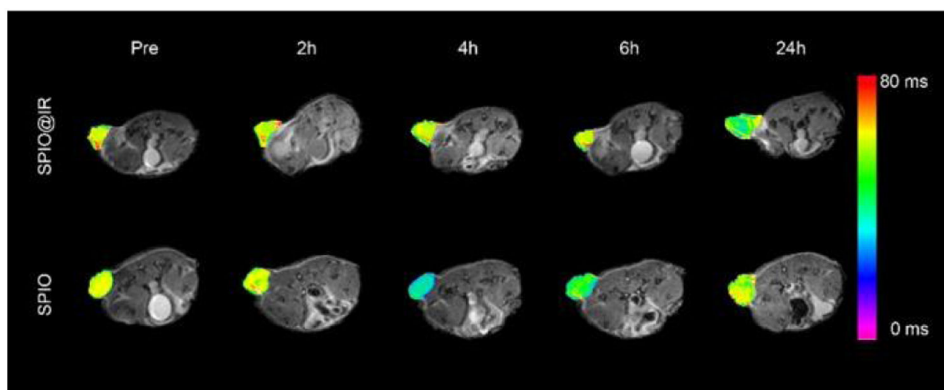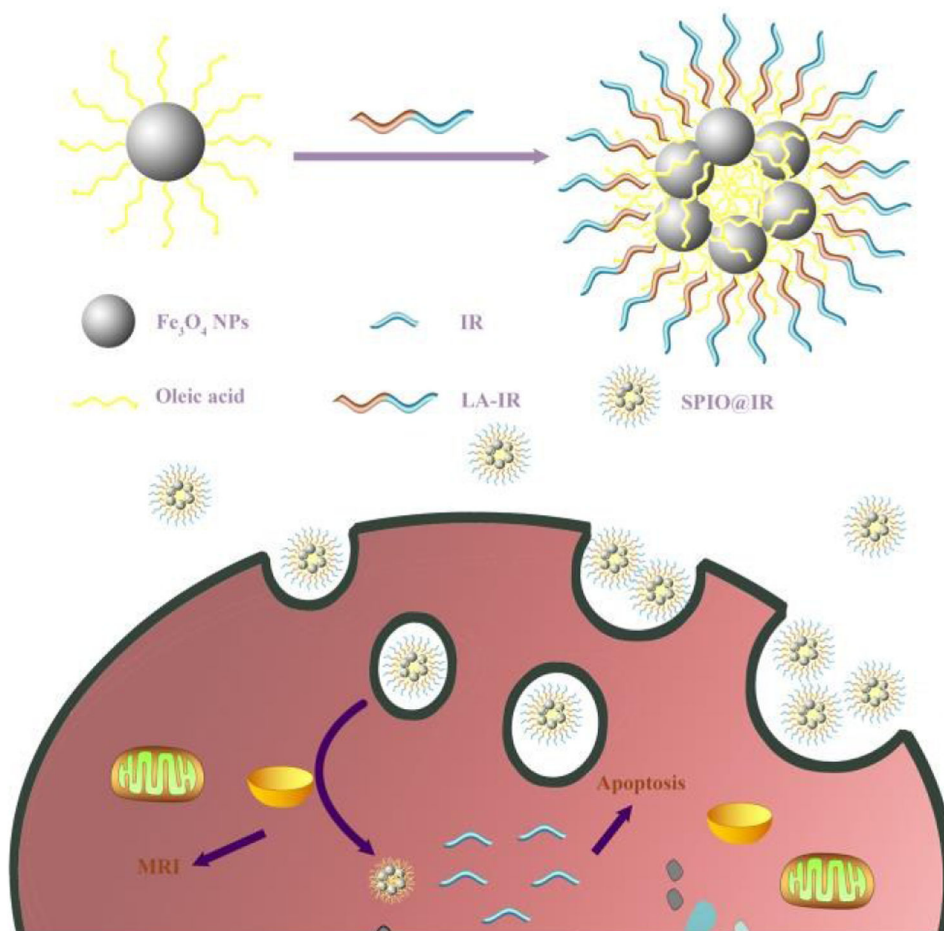
Fig.6.
T_2-Mapping images of colon cancer bearing mice pre-injection and at different time points post-injection of SPIO@IR and hydrophilic SPIO. Pseudocolors of T_2 mapping was used to highlight the difference between the two groups.

Scheme 1.
Schematic illustration of SPIO@IR based nanotheranostics in cells. Abbreviation: Fe_3O_4 NPs, superparamagnetic iron oxide nanoparticles; IR, Irinotecan; LA-IR, amphiphilic Laurie acid-lrinotecan prodrug; SPIO@IR, LA-IR inserted SPIO prodrug.